Carbon 168 (2020) 737–747

Contents lists available at ScienceDirect

Carbon

journal homepage: www.elsevier.com/locate/carbon

Ultrasonic exfoliation of graphene in water: A key parameter study

Anastasia V. Tyurnina [a, *], Iakovos Tzanakis [b, c], Justin Morton [b], Jiawei Mi [d], Kyriakos Porfyrakis [e], Barbara M. Maciejewska [c], Nicole Grobert [c, f], Dmitry G. Eskin [a]

[a] Brunel Centre for Advanced Solidification Technology, Brunel University London, Kingston Lane, UB8 3PH, UK
[b] School of Engineering, Computing and Mathematics, Oxford Brookes University, College Cl, Wheatley, Oxford, OX33 1HX, UK
[c] Department of Materials, University of Oxford, Parks Rd, Oxford, OX1 3PH, UK
[d] Department of Engineering, University of Hull, Cottingham Rd, Hull, HU6 7RX, UK
[e] Faculty of Engineering and Science, University of Greenwich, Central Avenue, Chatham Maritime, Kent, ME4 4TB, UK
[f] Williams Advanced Engineering, Grove, Oxfordshire, OX12 0DQ, UK

ARTICLE INFO

Article history:
Received 3 May 2020
Received in revised form
7 June 2020
Accepted 10 June 2020
Available online 29 June 2020

Keywords:
Ultrasonic exfoliation
Cavitation intensity
Few layer graphene
Ultrasonic frequency

ABSTRACT

Liquid Phase Exfoliation (LPE) is an efficient method for graphene flake exfoliation and considered to be compatible with industrial production requirements. However, most of available LPE methods require the use of harmful and expensive solvents for chemical exfoliation prior to mechanical dispersion of the flakes, and therefore an additional step is needed to remove the contamination caused by the added chemicals, making the process complex, costly, unsafe and detrimental to the environment.

By studying the effects of key ultrasonic LPE parameters, our study demonstrates the possibility to control the production and quality of few-layer graphene flakes in pure water in a relatively short period of time. The driving frequency of an ultrasonic source, a higher acoustic cavitation intensity and uniform distribution of the cavitation events in the sonicated volume are the key parameters for controlling the thickness, surface area and production yield of few-layer graphene flakes. The results are discussed in the context of mechanical exfoliation. This opens a direction for developing LPE into a cost effective, clean, environmentally friendly, and scalable manufacturing process for the next generation of two-dimensional nanomaterials for industrial-scale applications.

1. Introduction

Graphene is a remarkable, flexible two-dimensional (2D) crystal with excellent and unique functional properties, which makes it the most promising candidate for 2D nanotechnological applications [1–3]. Graphene utilization is, however, restricted to a large extent by the difficulties in producing high-quality flakes with large surface area. Among the existing preparation methods of graphene, there has been always a challenge in balancing quality, cost, scalability, purity and yield of the graphene flakes [4]. It has been shown [4] that the three existing methods (chemical vapor deposition, bottom-up synthesis and synthesis on silicon carbide (SiC)) have very high cost in production and low scalability. The original way of making graphene, known as mechanical exfoliation, has little chance to be scaled up to industry level. The two other methods (reduction of graphene oxide and liquid-phase exfoliation (LPE)) seem rather suitable for mass production and have become the primary methods for producing commercially available graphene.

Reduction of graphene oxide allows the material production of bulk quantities with high yield and reasonably low cost but the quality of the graphene is low due to the presence of defects [5–7]. On the other hand, LPE as a typical top-down technique has a relatively small yield with a considerable amount of unexfoliated graphite needed to be removed. However, high scalability and low cost make this technique suitable for producing graphene in bulk quantities [8–10] with the quality comparable to synthesized graphene film on metal or SiC surfaces [4]. According to a recent LPE study in Ref. [11] this method is becoming a popular technique for scalable production of graphene. It should be noted that the size of LPE graphene flakes (a lateral size or an area of the flake) is rather small (typically less or around 1 μm) [5–10]. However, for many important applications, graphene flakes may not be necessarily large in size, atomically thin and of perfect crystallinity [12]. From an industrial point of view, different kinds of graphene samples

* Corresponding author.
E-mail address: Anastasia.Tyurnina@brunel.ac.uk (A.V. Tyurnina).

https://doi.org/10.1016/j.carbon.2020.06.029

should be exploited for various applications. For example, adding thermally expanded graphite (prepared in the multistep process including LPE via ultrasonication) could increase thermal, fire and heat resistance as well as the thermal conductivity of epoxy composites [13]. Few-layer graphene (FLG) flakes of small size with developed surface have been used in inkjet applications in electric circuits [14–17], printed medical sensors [18], biosensors [19,20], or gas vapor sensor [21]. One of the important recent discoveries is that micrometre-sized graphene and FLG are promising for filtration application, e.g. converting seawater into drinking water [22,23]. Hence, LPE offers controllable graphene (FLG) production: with different flake shapes and sizes, different amounts and types of defects as well as highly developed surface and edges in order to meet the needs of various new applications, such as filters, biomarkers, ink, epoxy composites, etc [24].

There are, however, significant drawbacks in the currently used LPE methods that are typically based on the following [11,25]: (1) chemical treatment processing (involving the uses of high cost, harmful and polluting solvents or surfactants) to enlarge the space between graphite layers, followed by (2) application of external fields such as shearing or ultrasonication to exfoliate and spread the flakes in the solution; and frequently (3) graphene purification from chemical residues [11,25,26]. A recent review on LPE [11] emphasizes the need to produce graphene by using green and non-toxic dispersants. In this aspect, water is ideal and appealing, especially after graphene was recently proven to be hydrophilic [27], as an environment-friendly and low-cost dispersion medium [14,28]. A few reported studies on water-based LPE still used surfactants, polymer stabilizers or some specialized ingredients as an exfoliation medium [26–35], which are considered to be necessary for the dispersion of graphene flakes in water. For a long time, graphite was believed to be hydrophobic with a water contact angle of about 90° [36]. Since then, reported wetting properties of graphite and graphene remained under debate due to the contradictions and inconsistencies of the published results [27]. Later Li et al. [37] have estimated the value for clean graphite surface as 64°, and shown that the hydrophobicity of graphite and graphene is actually due to airborne hydrocarbon contamination. Recently, Belyaeva et al. [27] have concluded that the graphene-water interface is transparent to polar and dispersive interactions, showing that the wettability of single and bilayer graphene is noticeably higher than that of graphite. For the first time the measured contact angle of water on graphene was lower than 30°. So, the fact that FLG may be rather hydrophilic raises the question as to whether a surfactant is absolutely required to stabilize graphene in water [15,27,38]. To the best of our knowledge, only a few attempts have been reported where solely water was used for graphene exfoliation via ultrasonication. One of these studies showed that the process required long treatment time (>60 h) [39]. Some reported that an extra step of exfoliation in N-methyl-2-pyrrolidone (NMP), dimethylformamide (DMF), or vapor-assisted pre-treatment was also needed [14,40–42]. Generally, those steps are required to initiate the expanding of the graphite source, while the ultrasonic (US) processing in these approaches was used rather to maintain FLG flakes dispersion in the solution.

In this paper, we focus on ultrasound-assisted LPE technique, realized by means of commercially available industrial equipment. We used only ultrasonic cavitation technology in pure water-graphite solutions, as a single step process for graphene exfoliation. Similar approach to LPE was published in Ref. [35] and was performed by using unique custom-made equipment for a small volume of water–surfactants solutions. Here we present a clean, environmentally friendly, and potentially scalable manufacturing process for graphene exfoliation in pure deionized water (DIW) without any addition of chemicals. We confirm the presence of graphene by numerous characterization techniques. Our method is able to produce high-quality FLG flakes with few defects and no immediate evidence of oxidation. As Turner et al. [35] have pointed out, most of US based LPE studies lack the understanding on the fundamental mechanisms driving graphene exfoliation. Their work highlighted the importance of optimizing the US parameters, named as an inertial cavitation dose (ICD), which is a combination of time and the input power. The US processes, described here, are performed at ICD reflecting developed cavitation and at a constant (rather short, 2 h) time of treatment. Our main focus was on further identifying the key cavitation parameters that influence the final structure of FLG in water. The driving force of the LPE by cavitation is, as in other US-based slurry processes, the implosion of micrometre-sized, vigorously oscillating bubbles [43]. Those bubbles store a huge amount of potential energy. When they catastrophically collapse, the energy is instantaneously released to produce high-speed liquid micro-jets (in the range of 100–500 m/s) [44], high-pressure shock waves (up to 1 GPa) [45,46] and local hot spots up to 10^4 K [47,48]. Such process is repeated many thousands of times within a second and is considered to be the driving force of the exfoliation of the graphite layers. The cavitation bubbles can be of different size and lifetime, can act individually or as a cloud of bubbles that may significantly affect their dynamics [49] and can behave in a stable or transient manner depending on the acoustic pressure field developed [50]. These phenomena determine the cavitation process itself, and may also control the graphene exfoliation mechanism. Since it is not possible to control the individual bubble behaviour in such a chaotic and dynamic environment, the ultrasonication parameters are adjusted based on the collective behaviour of the bubble clouds and the corresponding pressure waves by monitoring the ultrasonication parameters. For example, the driving frequency (f) and the acoustic power (W) related to the squared vibration amplitude (A^2) determine the average bubble size and concentration, respectively. The cavitation development depends on the acoustic power ($\approx A^2 \times f^2$), and the cavitation intensity is proportional to the released bubble energy. Other process parameters include the graphite source, concentration of the tested suspension, surfactant presence, temperature (T) and treatment time, as well as the geometry of the US reactor. In this article we focus on the influence of US parameters such as set-up configuration, frequency and power on the graphene exfoliation process.

2. Materials and methods

Graphite powder (GP) from Alfa Aesar (LOT: B08Z019) was selected as the graphite source in our experiments. The average size of the graphite particles was about 70 μm as per specification by the manufacturer. DIW of the purity type 2 supplied by Lab Unlimited Carl Stuart group was used as a dispersing medium.

Three types of ultrasonic transducer systems were used for graphene exfoliation process. Two of them were ultrasound horns (sonotrodes), which were immersed into the water volume from the beaker top. The one shown schematically in Fig. 1a (Hielscher UP200S processor) had a 3-mm diameter Ti sonotrode (marked as 1), working at a frequency of 24 kHz with the maximum (when the sonotrode operated at 100% of the input power) peak-to-peak amplitude 210 μm. In this study, it was operated at 50% of power only. The second one had a similar sonotrode but 20 mm in diameter (Fig. 1b) attached to a Sonic Systems ultrasonic processor L500, working at 20 kHz, with the maximum (100%) peak-to-peak amplitude of 30 μm. It was operated at 25 and 100% of power. The main difference between the two set-ups was the diameter of the sonotrode (Ø, shown in Fig. 1). When using the same beaker geometry and liquid volume and maintaining the same US

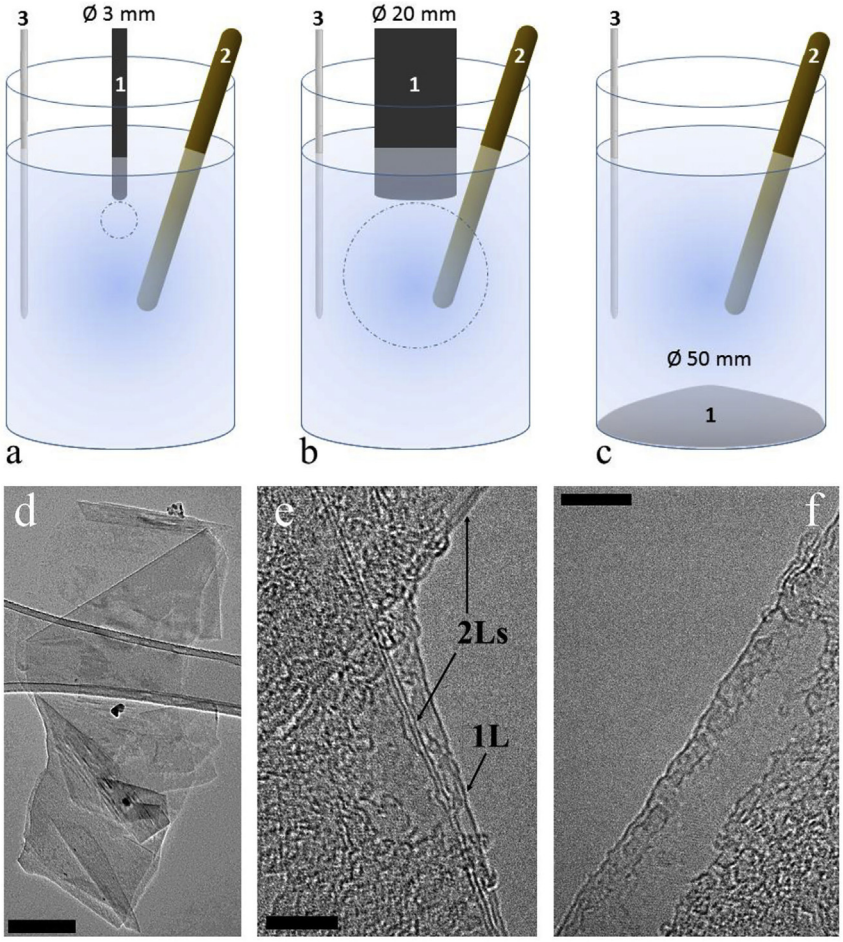

Fig. 1. Schematic view of the experimental set-ups. 3-mm (a) and 20-mm (b) sonotrodes immersed in the glass beaker (50 mm in diameter) containing DIW–graphite mixture; dashed line indicates cavitation zone size. When using a high-frequency membrane set-up instead of a sonotrode, the membrane is located at the bottom of the beaker (c), so the cavitation zone size spans over entire volume of the beaker. Numbers indicate a US source (1), a cavitometer (2) and a thermocouple (3). Typical images of the produced flakes: (d) low-resolution TEM image of one of the FLG flake after US exfoliation process and centrifugation, scale bar 200 nm; high-resolution TEM image of the same flake from (d): (e) edges of several bilayer graphene sheets (2Ls) overlapped with SLG (1L) are shown; and (f) the edge of SLG; (e, f) scale bar of 5 nm. (A colour version of this figure can be viewed online.)

parameters (cavitation intensity, temperature and time), the set-ups obviously differed by the cavitation zone diameters, indicated in Fig. 1a and b by the dashed line. The ratio of the cavitation zone (v) to the treated volume (V – water volume in the beaker) in the case of the 3-mm sonotrode is $v_{3mm}/V = 0.0003$, while for the 20-mm sonotrode it is $v_{20\ mm}/V = 0.1$. These ratios define the differences in the US energy distribution in the vessel bulk (discussed below). The third type was a multi-frequency membrane transducer (Meinhardt Ultrasonics) with an upside down geometry (Fig. 1c), where the ultrasound was applied from the bottom of the beaker at 50 and 97% of input power.

Due to the multi-function performance of the piezoceramic transducer and the configuration of the Ti diaphragm (50 mm in diameter, equal to the beaker diameter, (1) in Fig. 1c), we were able to establish cavitation conditions at four working frequencies, i.e. 208, 378, 992 and 1174 kHz. In this configuration the cavitation zone volume is the entire volume of the beaker, $v_3/V = 1$. All of the described US systems could be operated either in continuous or pulsed modes.

The broadband acoustic noise level generated by the cavitation zone was measured (in mV) using a calibrated cavitometer developed and produced by the Belorussian State University of Informatics and Radioelectronics [51]. For all configurations the cavitometer was immersed from the beaker top, (2) in Fig. 1a–c. The cavitometer consisted of a tungsten wave-guide probe with a diameter of 4 mm and a length of 500 mm connected to a piezoelectric receiver mounted within a metallic enclosure. A full description can be found elsewhere [51]. The signal acquisition and processing were carried out using a supplied acquisition system ICA-3M. Cavitation intensity (level of broadband noise) was registered as the full integral of the cavitation noise from all bubbles: pulsed stationary bubbles and transient bubbles that produced shock wave emissions (associated with MHz frequencies) upon their implosion.

As it is schematically shown in Fig. 1a and b, in the sonotrode configuration the US source (marked as (1) in Fig. 1) was submerged (2-mm below the liquid surface) into the central area of the mixture volume. In the membrane configuration (Fig. 1c) the US field was applied from the bottom. 150 ml of DIW were filled into a glass beaker of 50-mm diameter. 60 mg of the GP were added into the beaker and stirred manually with a Teflon spoon prior to ultrasonication to obtain mixture consistency. Three other initial concentrations of GP were used to analyse the yield dependency presented in detail in the supplementary information. The mixture was further ultrasonicated for 2 h under specific US parameters: cavitation intensity, frequency and transducer type. US field was applied under the input power of 25–100% depending on the US source, to initiate and to maintain the cavitation process. To ensure

comparable condition between different set-ups or when we varied one of the US parameters, we always maintained the similar cavitation conditions by monitoring and maintaining the same cavitation intensity (level of broadband noise). The measurements by the cavitometer were taken in the central region of the solution volume, approximately 3 cm away from the US source surface, (2) in Fig. 1a–c. During the first 15 min, the DIW slightly warmed up and then remained at ~ 40 °C for degassing process for further 10 min. Depending on the set-up, a cooling bath, fan or hot plate were applied to stabilize and maintain the same temperature at 40 ± 3 °C. The reason for choosing this temperature is the fact that it seems to promote long-term stability of dispersed graphene [39], and is similar to that in the studies yielding of high quality graphene [52,53]. During the ultrasonic processing, a standard K-thermocouple with an RS 52 Digital Thermometer was used to monitor the temperature of the mixture ((3) in Fig. 1a–c).

After US processing, the water solution became dark black and was further centrifuged (CF) for 30 min at 1500 relative centrifugal force (rcf) using a Heraeus Labofuge 400R system. The upper part of the CF solution was separated at once in order to prepare several different supernatant samples for advanced characterization.

First, a UV–vis spectroscopy (a UV spectrometer by Hewlett Packard 8453) was used to identify the solution composition. For that, a certain amount of the CF solution was poured into a 3.5-ml Cole-Palmer quartz cuvette and measured immediately to avoid partial agglomeration of the flakes and their sedimentation (precipitation) in the aqueous solution. Each UV–vis spectrum was collected with an acquisition time of 10 s in the spectral range from 220 to 800 nm, to cover the range where graphene and GO related peaks are expected to be seen.

Consequently, one drop of the CF solution was transferred onto a cleaned Si/SiO_2 (300 nm) surface and dried at room temperature (RT) within a ducted fume cupboard prior to Raman investigation. Another 3 drops were put onto holey-carbon-coated copper grids (300 mesh) for transmission electron microscopy (TEM) investigation and also dried at RT. Both dried samples were stored in plastic wafer-trays to be measured some days later. An InVia Raman (Renishaw) spectroscopy system with Modu-Laser working at an excitation wave length of 514 nm was used to confirm the FLG structure, to verify the number of layers (NLs), presence of defects, and to trace the graphite flakes structure quality after US process. The laser spot size was ~ 2 μm and the laser power was 0.2 mW. Raman spectrum of 20–30 random flakes were registered in the range from 1200 to 3100 cm^{-1}. Data collection was carried out at 50 × magnification, the acquisition time was adjusted to have a reasonable signal/noise ratio.

A high-resolution 200-kV JEOL 2100F Field Emission Gun TEM was used to investigate individual FLG flakes in terms of their area and NLs. One of the TEM investigated FLG flake is illustrated at low magnification in Fig. 1d. The fragments of bilayer and single layer graphene (SLG) are shown in high-resolution TEM images (Fig. 1e and f). 20–30 representative flakes were investigated for each of the US conditions. Further image processing was performed with ImageJ software in order to estimate the surface area and thickness of each flake.

3. Results and discussion

Prior to the investigation of the effect of the US parameters, Raman spectroscopy was used to characterise the original graphite source in comparison to the FLG flakes exfoliated by different US sources, but under the same experimental conditions: duration, temperature and input power. Fig. 2 summarizes the results. All obtained spectra (Fig. 2a) always contained four main Raman features typical of a well crystallized sp^2-hybridized carbon material [54–56]: G band around 1580 cm^{-1}, defect-related modes (D and D′) around 1350 cm^{-1} and 1620 cm^{-1}, respectively, and the second order Raman scattering (2D) peak around 2700 cm^{-1}. Typical Raman spectra of FLG flakes obtained after US treatment (Fig. 2a, spectra in black (1–3)) repeat the bands positions, width and shape of the spectrum in grey (4) of the original graphite material, but showing bigger 2D to G intensity ratio suggesting that they are thinner than the original GP particles [57]. Intensity ratios between the Raman peaks D, D′, 2D and G of the spectra from different US set-ups are collected in Table S1.

It should be noted that some spectra of the as-produced FLG flakes were typical of those of low defective SLG where 2D to G intensity ratio was bigger than 1, the D to G intensity ratio was close to that of original GP and the 2D shape was symmetrical with the peak width smaller than 25 cm^{-1} [54,64] (2D peak width of the rest of the examined flakes was more than 60 cm^{-1}). An example of a typical Raman spectrum of SLG, produced in this work, is presented in Fig. 2b.

A comparison of the original GP spectrum with the spectra of FLG flakes prepared by 2 of US set-ups (50-mm membrane at 1174 kHz and 20-mm/20-kHz) generally did not show significant quality degradation (see D/G and D′/G ratios data in Fig. 2c for power 50%). It is worth noting that the spectra of FLG produced by the membrane US set-ups have shown the smallest D/G and D′/G intensity ratios (for both of tested powers), see Spectrum 3 in Fig. 2a, data in Fig. 2c (grey diamond and triangular symbols) and Table S1. The higher noise level in the case of Spectrum 3 of Fig. 2a can be explained by the smaller crystal size. This is expected since the Raman peak intensity is proportional to the volume of the sample.

Based on this we can assume that the highest frequency membrane set-up is a “gentler” approach towards US treatment for FLG exfoliation. The defect-related modes (D and D′) in Spectrum 1 (Fig. 2a) and so the D/G and D′/G ratios data in Fig. 2c at 50 % of power (open diamond and triangular symbols) was significantly greater (Table S1), meaning that FLG samples after exfoliation by the 3-mm sonotrode became more defective compared to the original graphite source and to the FLG flakes obtained by other US set-ups. It is known that D/D′ intensity ratio can be used to quantify the defects in graphene [58]. In our experiment D/D′ ratio for the flakes, exfoliated by any US set-up (Spectra 1–3 in Fig. 2a), was smaller than that of original GP, i.e. less than 1.75 (Table S1). Given that, we can assume that our sonication processes do not introduce any significant number of basal plane defects [35,58] and may conclude that the observed increase in amount of defects is more due to the thinning of the graphite flake and its size decrease [35,58,59].

3.1. Effect of US configuration geometry

To understand the importance of US configuration geometry, we firstly performed exfoliation under the same cavitation intensity using two horn-type US systems; both at a frequency around 20 kHz. In the case of the 3-mm sonotrode ($v_{3mm}/V = 0.0003$), the US field is more heterogeneous, with acoustic energy releasing close to the tip of the sonotrode, forming a very concentrated cavitation zone expanding downwards in a typical conical structure that quickly attenuates due to the shielding effect [49], with, therefore, “dead zones” in the vessel farther away from the tip. In the case of the 20-mm sonotrode, the cavitation zone volume is comparable on the same scale to the treated volume in the beaker ($v_{20\ mm}/V = 0.1$) and, with taking into account the secondary acoustic flows [60], the entire volume issubjected to treatment. These differences in set-up configuration result in different conditions for graphene LPE. To verify this effect, we prepared the FLG

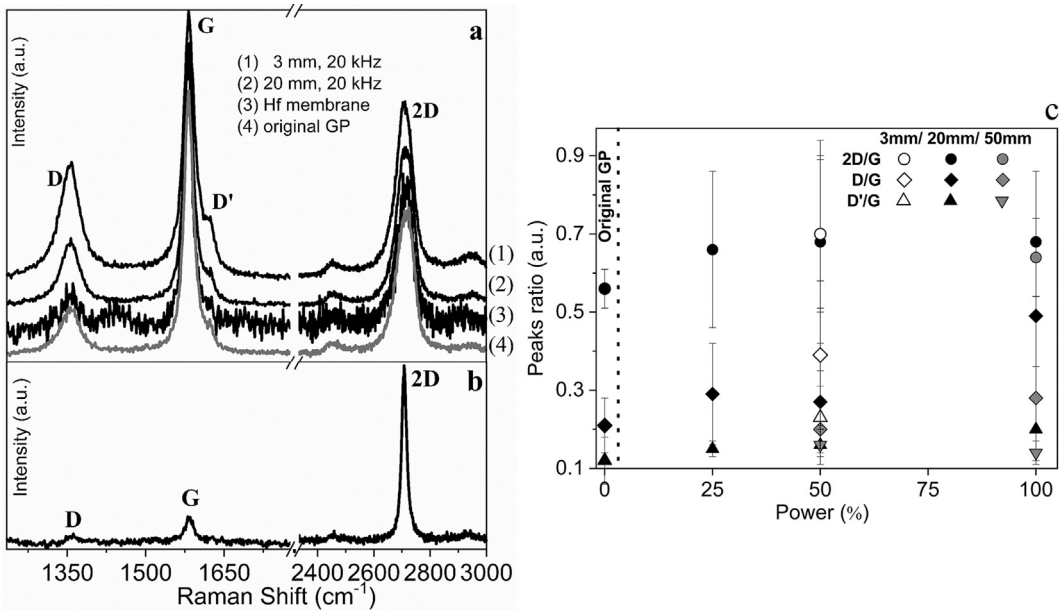

Fig. 2. (a) Averaged Raman spectra of the FLG flakes after US processing with different set-ups (1–3) and the spectrum of the original graphite material (4), spectral intensities are normalized by the intensity of the G mode at 1580 cm^{-1}. The names of the main peaks are indicated; (b) An example of a Raman spectrum registered for one of SLG flakes obtained after US exfoliation process. (c) Different Raman peaks intensities ratios (2D, D, D′ to G) for all used US configurations vs input power. The data at zero power (separated by dashed line) correspond to the Raman data of original GP. 3 mm, 20 mm and 50 mm are the indications for US set-up with corresponding size of the US source.

flakes solution using the 3 and 20-mm sonotrodes under the same US conditions, i.e. cavitation intensity as measured by the cavitometer and the input power integrated over the sonotrode tip area ~ $2\pi\rho c \times f^2A^2 \times \pi\text{Ø}^2/4 \cong 3$ kW [61] for maximum amplitude, where ρ - water density, c - US velocity in water). The obtained aqueous solutions of FLG flakes were then characterized by means of UV–vis, Raman spectroscopy and TEM.

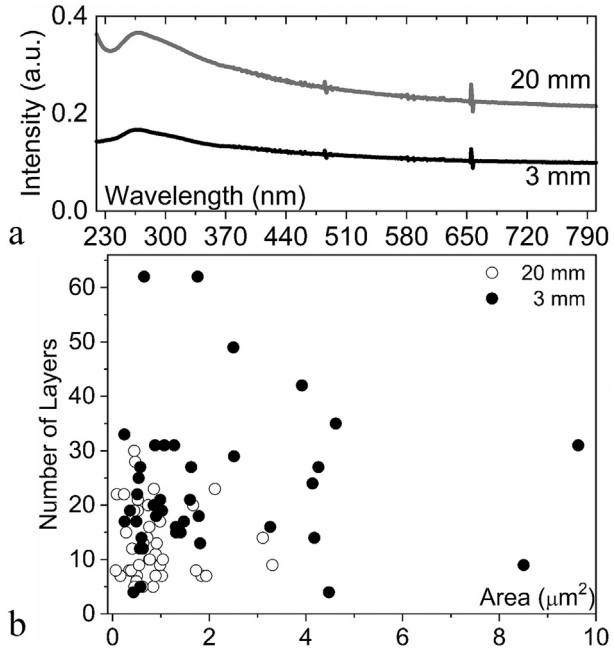

Fig. 3. Characterization of FLG flakes produced by two sonotrodes of different diameters. (a) UV–vis spectra for as-obtained FLG flakes solutions; (b) TEM data presented as the surface area and NLs distribution for each examined flake. Corresponding diameters of the sonotrodes are indicated at the graph.

The corresponding UV–vis spectra are displayed in Fig. 3a. The shape of each spectrum was identical to a typical spectrum of graphene, i.e. characterized by a pronounced peak around 270 nm attributed to the presence of graphene [62,63]. We did not observe the peak around 230 nm related to the presence of graphene oxide [64,65], indicating that the as-obtained FLG flakes were not oxidized up to the level that can be detected by UV–vis. A lower peak intensity for the as-treated sample obtained with the 3-mm set-up was apparently due to a lower concentration of FLG flakes.

Raman spectroscopy investigation of the samples after US revealed two clear features (see spectra 1 and 2 in Fig. 2a and data in Table S1): in the case of the 3-mm sonotrode the intensity of the D′ peak around 1620 cm^{-1} (or the corresponding D′/G intensity ratio in Fig. 2c) was higher; and D to G peak intensity ratio in Fig. 2c (Table S1) was bigger. The D′/G intensity ratio increase implies a larger amount of edge defects in the crystal structure (so-called edge states) [55,56]. The D to G peak intensity ratio is related to the defect amount in the crystal [54–56]. Given that, we can conclude the following: FLG flakes after US treatment with the 20-mm sonotrode were of better quality, i.e., with fewer defects, as compared to the samples obtained with the 3-mm sonotrode (open and black diamonds symbols in Fig. 2c at 50% of power). This can be related to the fact (discussed above) that the 3-mm sonotrode created a concentrated cavitation zone of rather high acoustic intensity, which was destructive for graphite flakes. Probably GP fractions under that high-intensity were rather breaking perpendicular to the graphite planes than thinning via splitting the graphitic layers, which is confirmed by the biggest observed value of D′/G ratio, related to edge defects (open triangular symbol in Fig. 2c).

Finally, the as-obtained FLG flakes were investigated by TEM. Typical TEM images of the FLG at low and high-resolution are presented in Fig. 1d–f. The analysed TEM data is summarized in Fig. 3b as the distribution of individual flake sizes and thicknesses (number of layers) for each set-up. The graphite flakes obtained

after US with the 3-mm sonotrode had a wider variation in NLs and area (black dots in Fig. 3b) while the 20-mm set-up allowed us to produce thinner FLG flakes with the surface area up to 3 μm^2 (black open circles in Fig. 3b). That could be again related to the fact that the 3-mm sonotrode created a non-uniform US field in the vessel, which led to a wider variation in the thickness and size of the exfoliated flakes. Corresponding flakes were also more defective (Fig. 2a,c and Table S1) than the initial graphite source, while their concentration in the solution after centrifuging was very low, according to the UV data in Fig. 3a. The average thickness of the flakes exfoliated by the 20-mm sonotrode was 14 Ls, which is half as thick as flakes prepared by the 3-mm sonotrode. So in the latter case most of the flakes could not be called as FLG.

Note that the overall level of the broadband noise (reflecting the overall emissions from cavitation bubbles) was kept the same in both cases but was obviously generated by two very different distributions of cavitation events, i.e. very locally concentrated cavitation zone in the case of the 3-mm sonotrode and more uniformly distributed cavitation region in the case of the 20-mm sonotrode. The size of the cavitation zone is about 1.5 of the sonotrode diameter [66], implying a difference of 4.5 and 30 mm in the diameter of the active cavitation zone among these 2 US tip set-ups (as illustrated schematically in Fig. 1a and b). Therefore, the 20-mm sonotrode generates a cavitation zone that covers almost all treated volume, especially if the acoustic streaming and re-circulated acoustic flows are taken into account [60]. The tested set-up configurations demonstrated also the importance of the ratio between the diameters of the sonotrode (3 or 20 mm) and the beaker (50 mm). So the US field distribution along the solution volume was getting more uniform when those diameters were closer to each other. The uniform cavitation treatment provided more uniform FLG flakes size and thickness distribution (TEM results in Fig. 3b) as compared to the set-up with a concentrated cavitation zone. Moreover, the smaller sonotrode but with the same input power generated higher cavitation concentration in a smaller volume, resulting in more defective structure of the final FLG flakes.

3.2. Effect of excitation frequency

In addition to different sonotrode diameters, we further investigated the frequency effect on the exfoliation process using two US set-ups covering the frequency range from 20 (20-mm sonotrode) to 1174 kHz (50-mm membrane). In order to make sensible comparison for different types of oscillating sources, we maintained the broadband acoustic noise level at the same value in mV for each of the tested regime, which was achieved for each frequency by adjusting the input power of the ultrasonic generator. In all experiments the temperature was in 40 ± 3 °C over 2 h of processing. To assure this, the highest frequency set-up was used in a pulse mode, otherwise the temperature would increase higher than 40 °C. UV–vis spectra of all as prepared samples (Fig. 4a) demonstrated a standard FLG related peak of different intensity in UV range around 270 nm, except for the sample from 208-kHz set-up (spectrum no 3). A sample obtained under 208 kHz sonication exhibited a sharp peak at ~250 nm, untypical of graphene suspension. That must be due to a lower cavitation intensity (per volume) that was introduced during US processing in order to maintain the given broadband noise level in our experiment, i.e. smaller amount of bigger bubbles. The cavitation pressure generated by these bubbles and distributed over entire volume apparently was not sufficient to reach effective cavitation-driven exfoliation. So the exfoliation rate was low due to inadequate combination of cavitation bubble concentration, size and activity. The lowest UV absorbance rate was observed for the samples exfoliated at 992 and 378-kHz set-ups (number 1 and 2 spectra, respectively). The highest peak intensities in Fig. 4a (spectra number 5 and 4, respectively) were observed for FLG flakes solutions obtained under 20 and 1174-kHz US treatment. Given that, we can assume that those set-ups provide FLG flakes solution of higher concentration as compared to other tested frequencies.

Raman spectroscopy study did not show significant differences between the spectra of the samples exfoliated under different frequencies, except for the sample prepared by US process at 208 kHz, for which significantly higher Raman intensities were observed for defects related peaks (D and D′ to G ratios in Table S1). Based on the spectral analysis of Raman data (main peaks positions, ratios and width) we can conclude that the resulting material is thin graphite flakes (2D/G ratios were greater than those of original GP [57]) with low amount of defects: D/G and D′/G ratios were slightly bigger than those observed in the spectra of original graphite source (Table S1) [55,56]. Nevertheless, when looking at D/D′ ratio, which was not greater than 2, we can assume that those defects are rather edge defects [67], which appear due to the reduction of flake size and thickness [59]. This shows that for FLG flakes the sono-exfoliation processes went without introducing a notable number of basal plane defects, thus, we can exclude the quality degradation during US processes used. It should be noted that the intensity ratios D/G and D'/G (see Table S1) of the samples obtained using the membrane at the highest frequency were the smallest, which indicates their better quality compared to the FLG flakes produced by the same US set-up but at lower frequencies. As one can see in Fig. 2c, grey diamond and triangular symbols at 100% power are slightly lower than those in black colour at 25% of power. Thus, the higher the frequency set-up is, the “gentler” the US treatment will be.

Fig. 4b gives the summary of TEM results for the size and thickness distribution of individual flakes. The inset summarizes these data as the average value for each frequency with the standard deviation. As one can see, for the sample solution prepared at 208 kHz we were able to find only few FLG flakes (with thickness lower than 10 Ls) on the TEM grid. Size and thickness distributions (squares in Fig. 4b) with an average thickness of 31 Ls (Table S1) of all examined flakes produced using this frequency were highly variable. This is in good agreement with our hypothesis that the exfoliation in this regime was not as effective as in the other investigated US regimes. For the samples obtained using other frequencies their values were spread within the same region, indicated by the dashed rectangular in Fig. 4b. Looking at the plot of the average data one can find that the distribution was similar only for the surface area, within the range of 1–3 μm^2. FLG flakes obtained in the 20-kHz set-up showed larger NLs (15 on average), while the higher frequency membrane set-up produced the FLG flakes with the average NLs lower than 10 (see Table S1), the thinnest flakes were detected for the highest frequency US set-up (~ 7 Ls on average). Thus, the higher the frequency, the thinner the graphite flakes. It is also important to recall that FLG concentration (quantity of exfoliated flakes in solution) in the water is one of the main characteristics for further application and mass production. The UV–vis investigation demonstrated that the 20-mm/20-kHz sonotrode set-up provided us with the FLG solution of the highest concentration. The next highest concentration was detected for the membrane working at highest frequency 1174 kHz (Fig. 4a, spectra 4 and 5).

3.3. Effect of input power

Results from experiments related to the effect of excitation frequency were obtained by maintaining the level of broadband noise generated by cavitation bubbles (cavitation intensity) for all five frequencies. That was achieved by adjusting the input

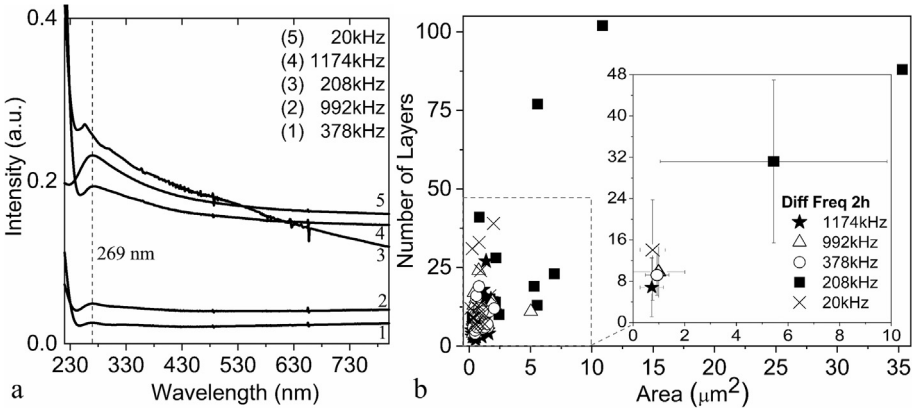

Fig. 4. Characterization of FLG flakes produced at different frequencies. (a) UV–vis spectra for as-obtained FLG flakes solutions; (b) TEM data presented as the surface area and NLs distribution for each examined flake. Inset presents the average data of the main plot with their standard deviations. Corresponding frequencies are indicated in the graph legend by number for UV–vis data, by symbol for TEM results.

transducer power for each set-up, so that the highest transducer power was required for the highest studied frequency of 1174 kHz. In this section we analyse the effect of input power on the cavitation process and FLG flake production. For the minimum (20 kHz - Lf) and maximum (1174 kHz - Hf) frequency set-ups, that have shown the best results for FLG exfoliation, we repeated the US exfoliation process at different input power levels and characterized the produced solutions in the same way as described above (sections 3.1 and 3.2). So for the 20-kHz sonotrode the US process was performed at three different powers, i.e., 25, 50 and 100 % and for the membrane configuration at a frequency of 1174 kHz it was conducted at 50 % and 97 %, meaning that cavitation intensity was increased with input power value. A lower input power for Hf process did not provide sufficient level of cavitation and FLG exfoliation.

Raman spectroscopy confirmed the graphitic structure of the final FLG flakes. According to the data presented in Fig. 2c, the 2D/G intensity ratio was bigger than that of the original graphite source (Table S1). The quality of as-prepared samples was comparable to the quality of the pristine graphite source (D/G and D'/G intensity ratios in Fig. 2c and Table S1). Although for the Lf US set-up at the maximum input power a sufficient increase (almost doubled) of the average D/G intensity ratio was detected, leaving another ratio D'/G, also related to defects, almost unaltered. Since the D/D' intensity ratio increased to almost 2.5, we suggest that the 20-mm/20-kHz US process at 100 % power may introduce some basal plane defects [58,67].

The analysed TEM data are accumulated in Fig. 5a and b as the surface area and NLs distribution for each examined FLG flake. A common behaviour for both configurations was observed in the presented distributions. For each set-up the rising of the input power led to enlarging of the flake area and reduction in the flake thickness (transit from open/grey to black circles). The average of the main data, plotted in the inset of Fig. 5b, revealed that at 50 % power the Hf membrane set-up produces thinner, more uniform but smaller in size FLG flakes than flakes exfoliated under the same power of the Lf set-up. The Lf process leads to obtained FLG flakes of slightly larger area at any power. The thinnest and largest FLG flakes were observed at maximum power of the 20-mm sonotrode: the thickness reduced down to 5 Ls on average (Table S1) and the flake area up to 5 μm^2 (black circles in Fig. 5a), which was not reached using the membrane US set-up (black circles in Fig. 5b). Worth noting that due to the different US sources geometry (see section 3.1), for the same input power the cavitation intensity was several times lower in case of Hf set-up. So the cavitation intensity was comparable only for processes in Lf set-up at 25 % of power and in Hf set-up at 100 % of power. An interesting conclusion can be made from the UV–vis analysis of the same samples. For both US configurations the intensity of the peak related to graphene presence rose up with increasing the input power (Fig. 5c and d).

The yield of dispersed FLG flakes production was estimated following the procedure described elsewhere [35]. The highest yield of 12.5 % was achieved in the configuration with 20-mm/20-kHz sonotrode. This number is comparable to the results of Turner et al. (16 %, Fig. 3a in Ref. [35]), where the same frequency US process in aqueous solutions, although with sodium cholate as a surfactant, was used. However, as we show in Supplementary Materials the yield strongly depends on the centrifugation rate (Fig. S1), which was intentionally chosen to be low by Turner et al. [35]. Moreover, our FLG flakes exfoliated only in DIW were of similar average thickness (5–6 Ls), but of larger average area by more than 150 times (~2.5 μm^2 in the current work vs ~0.015 μm^2 in Ref. [35]). The quality of our FLG flakes also seems to be better in terms of the defect amount introduced after US process. Firstly, the average D/G peak intensity ratio increased from ~ 0.08 for original graphite (Fig. S4.3 in Ref. [35]) to ~ 0.47 for all samples treated during 2 h in the reference (see Fig. 4 in Ref. [35]). The average D/G peak intensity ratio in our work was ~ 0.3, which is closer to the one of original graphite powder (0.21) (Table S1). Secondly, the D/D′ intensity ratio (Table S1) was below 2.5 in our work and ~ 3 in Ref. [35], hence, we also can conclude that our FLG flakes are less defective, and most of the defects are edge related [58].

3.4. Sono-exfoliation mechanisms

The mechanisms for the sono-exfoliation of graphite are closely related to the established cavitation regime. The size, distribution and collapse of bubbles as well as their number and spatial distribution are important parameters, which in turn are controlled by frequency, power, and set-up configuration geometry. By varying frequency in our US set-ups, we did not observe any significant changes in the quality of as-produced FLG in terms of amount of defects, which were monitored by the Raman intensities ratios D/G and D′/G. Based on TEM investigation, a clear thickness dependency on the driving frequency was noticed: the higher the frequency, the thinner the FLG flakes under similar cavitation intensity. The well-known Minnaert equation [68,69] predicts that the bubble linear resonance size (when the bubble becomes unstable and implodes) depends on the acoustic frequency and in water at ~ 20 kHz it is ~ 138 μm while at 1174 kHz should be around ~ 2 μm [70].

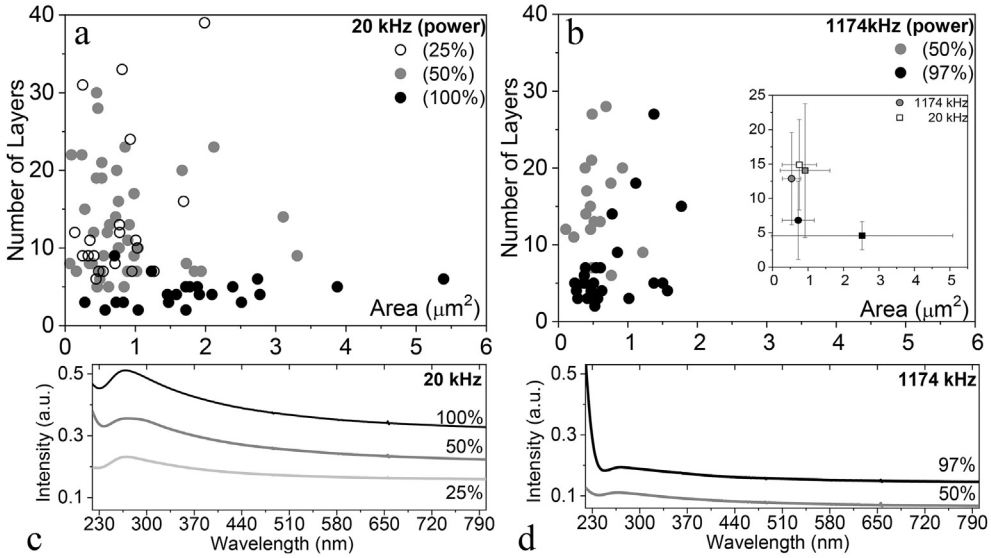

Fig. 5. TEM data presented as the surface area and NLs distribution for each examined flake in dependence on the input power and set-up: the 20-mm sonotrode working at 20 kHz (Lf) (a); the 50-mm membrane working at 1174 kHz (Hf) (b). Power level and corresponding frequencies are indicated at the top right corner of each graphs. Inset represents the average area and thickness data for both US set-ups: circles use for Hf, square - for Lf; colour corresponds to the different input power and same as on the main plot, Fig. 5a and b. Corresponding UV–vis spectra of as-obtained FLG solutions for each US process: (c) is for 20-kHz/20-mm sonotrode, (d) one is for 1174-kHz/50-mm membrane.

Additionally, bubbles in that range have the tendency to collapse under right/resonant conditions as shown in Ref. [71] producing liquid jets in the nanometer range. Typically liquid jet tip is in the range of 1/10th of the maximum or resonant bubble radius as experimentally showed in Ref. [72].

Additionally, due to the chain reaction of cavitation bubble multiplication [73], the first collapse is accompanied by the formation of even smaller in size bubbles (nanobubbles [74]). Although the nanobubbles produced in the chain reaction are significantly larger (over 30 nm [74]) than the interlayer graphite gap, they are still excited by the shock waves or even the incident frequency of 1174 kHz so they can vigorously oscillate generating different vibrating modes the so-called “Faraday or surface waves” [75]. As the surface waves of MHz frequency resonate, they form unstable and highly non-linear/chaotic and dynamic structures [76]. Bubble pressures may reach a few hundreds of kPa [75,76] adequate to exfoliate the layers as reported in elsewhere [77]. Based on this, we assume that the high-frequency US treatment described here was “gentler” in terms of size of jets emitted due to the vigorous contraction or implosion action and was more suitable for exfoliation in terms of cavitation bubble sizes. Petrier et al. [78] observed that the size of the collapsing bubbles and the duration of the collapse decreased with the increasing frequency. Given that, the membrane US configuration seems to be rather suitable for higher quality graphene exfoliation. On the other hand, the 20-mm sonotrode at 20 kHz produces larger bubbles that collapse more violently and may be more effective in dispersing the flakes, leading to higher concentration of FLG in solution as seen in Figs. 4a and 5c,d but also generating large amount of smaller cavitation bubbles. It was suggested that the bubbles of micrometre size can break the graphite particles in the direction perpendicular to graphitic planes while the smaller bubbles expand gently the space along the layers [79].

A combination of these two approaches of exciting cavitation seems promising to industrial scale-up, which is in line with the results reported elsewhere [28]; though the authors of ref. [28] used a combination of a 30-kHz bath and a 20-kHz sonotrode with surfactants and chemical exfoliating agents.

An alternative mechanism of cavitation-induced exfoliation in water is based on sonochemistry. According to Kim et al. [39] layer-by-layer graphene exfoliation in water occurs solely due to a sonochemical reaction of the free radicals produced by the bubbles collapsing. They performed the ultrasonication at two temperatures (30 and 60 °C) in a 40-kHz US bath for 60 h (!) and concluded that cavitation achieved only at 60 °C was responsible for the observed exfoliation. Unfortunately, the provided data was related to the chemistry only and the analysis of the US parameters and cavitation was not done properly.

Our ongoing research on in-situ observations of graphene exfoliation under cavitation treatment gives us confidence in the physico-mechanical mechanisms of exfoliation. Using high-speed filming of exfoliation we observed splitting of graphite flakes by oscillating and imploding bubbles. These observations and their analysis are the subject of a forthcoming publication and the reader is directed to Ref. [77] for details. Here we just illustrate the suggested mechanisms by a sequence of frames obtained at a rate of 100,000 frames per sec using FASTCAM SA-Z type 2100K-M. The same 24-kHz 3-mm source of ultrasound was used in pure water and a graphite flake was fixed to the glass vessel bottom. Fig. 6 clearly demonstrates how the cavitation bubbles generated at the sonotrode tip, are splitting the graphite flake and then gradually exfoliating the flake by continuous penetration of the bubbles into the opening between the graphite layers.

4. Conclusions

We studied the effects of the key ultrasonic LPE parameters, i.e. frequency, configuration geometry and power, on the quality, size and yield of FLG flakes produced in DIW without any additions of chemical surfactants in a limited period of time (2 h) in a 50-mm diameter vessel with 150 ml of water-powder solution at 40 °C. A uniform distribution of cavitation events throughout the treated volume assisted by primary and secondary acoustic flows was a key factor in producing good quality FLG flakes.

The best results in terms of larger in surface (~ 1–3 μm^2) and thinner in size (~ 5 layers) FLG flakes were obtained with a sizable

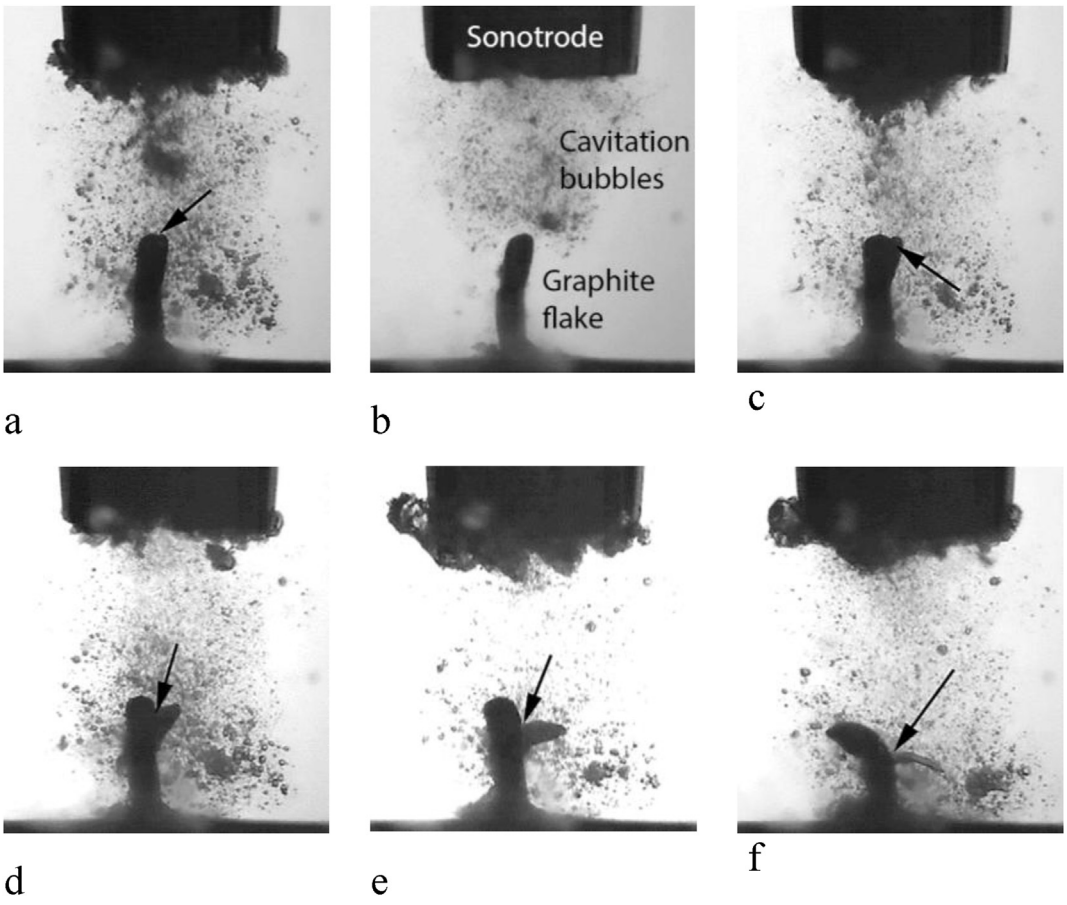

Fig. 6. A high-speed sequence (from a to f) of frames illustrating physico-mechanical exfoliation of a graphite flake by a 24 kHz 3-mm ultrasonic source. Arrows show the place of splitting (exfoliation) with cavitation bubbles penetrating the split. 100,000 fps using FASTCAM SA-Z type 2100K-M. The supplementary video can be accessed with the online version of the article as Video 1 (Suppementary material 1).

(20-mm) sonotrode at 20 kHz and with an oscillating membrane (50-mm) at 1174 kHz. To the best of our knowledge and based on the comparison with the very recent research findings in this field, we can conclude that our results are on par with the best results for graphene sono-exfoliation in water. A combination of two frequencies of sonication might be promising for practical implementation of LPE without harmful additions. The increase in the input power reduces the average thickness of the final FLG flakes and improves the yield of cavitation-induced LPE at both frequencies. Some parameters (uniformity in thickness and yield) still can be and should be further improved.

The suggested mechanism of FLG flakes exfoliation in water is based on the mechanical action of small active cavitation bubbles that promote exfoliation and dispersion of FLG flakes. This mechanism is supported by the ongoing unique in-situ direct observations.

Future work will be directed towards combination of different ultrasonic sources and in-situ observations of cavitation-driven LPE with the aim to elucidate further the governing mechanisms.

CRediT authorship contribution statement

Anastasia V. Tyurnina: Conceptualization, Data curation, Methodology, Formal analysis, Investigation, Visualization, Writing - original draft. **Iakovos Tzanakis:** Conceptualization, Funding acquisition, Data curation, Writing - review & editing. **Justin Morton:** Investigation, Data curation, Visualization. **Jiawei Mi:** Funding acquisition, Writing - review & editing. **Kyriakos Porfyrakis:** Funding acquisition, Writing - review & editing. **Barbara M. Maciejewska:** Writing - review & editing. **Nicole Grobert:** Funding acquisition, Writing - review & editing. **Dmitry G. Eskin:** Conceptualization, Methodology, Funding acquisition, Project administration, Resources, Supervision, Writing - review & editing.

Declaration of competing interest

The authors declare that they have no known competing financial interests or personal relationships that could have appeared to influence the work reported in this paper.

Acknowledgments

This study is a part of the project “Sustainable and industrially scalable ultrasonic liquid phase exfoliation technologies for manufacturing 2D advanced functional materials” (EcoUltra2D) funded by the UK Engineering and Physical Sciences Research Council (EPSRC) under the grant nos. EP/R031665/1; EP/R031401/1; EP/R031819/1; EP/R031975/1. NG also thanks the Royal Society.

Supplementary Data

Supplementary data to this article can be found online at https://doi.org/10.1016/j.carbon.2020.06.029.

References

[1] E. Han, J. Yu, E. Annevelink, J. Son, D.A. Kang, K. Watanabe, et al., Ultrasoft slip-mediated bending in few-layer graphene, Nat. Mater. 19 (2020) 305–309, https://doi.org/10.1038/s41563-019-0529-7.

[2] K. Kanahashi, M. Ishihara, M. Hasegawa, H. Ohta, T. Takenobu, Giant power factors in p- and n-type large-area graphene films on a flexible plastic substrate, npj 2D Mater. Appl. 3 (6) (2019) 44, https://doi.org/10.1038/s41699-019-0128-0.

[3] J. Stone, Hybridizing graphene and photonic crystal fibre, Nat. Photon. 13 (2019) 731–732, https://doi.org/10.1038/s41566-019-0541-0.

[4] R. Raccichini, A. Varzi, S. Passerini, B. Scrosati, The role of graphene for electrochemical energy storage, Nat. Mater. 14 (2015) 271–279, https://doi.org/10.1038/nmat4170.

[5] J.H. Warner, F. Schäffel, A. Bachmatiuk, M.H. Rümmeli, Graphene: Fundamentals and Emergent Applications Ch, vol. 4, Elsevier Inc, Waltham, 2013, pp. 129–227.

[6] D.R. Dreyer, S. Park, C.W. Bielawski, R.S. Ruoff, The chemistry of graphene oxide, Chem. Soc. Rev. 39 (1) (2010) 228–240, https://doi.org/10.1039/b917103g.

[7] S. Park, R.S. Ruoff, Chemical methods for the production of graphenes, Nat. Nanotechnol. 4 (2009) 217–224, https://doi.org/10.1038/nnano.2009.58.

[8] M. Cai, D. Thorpe, D.H. Adamson, H.C. Schniepp, Methods of graphite exfoliation, J. Mater. Chem. 22 (2012) 24992–25002, https://doi.org/10.1039/C2JM34517J.

[9] K.R. Paton, E.V. Varrla, C. Backes, R.J. Smith, U. Khan, J.N. Coleman, et al., Scalable production of large quantities of defect-free few-layer graphene by shear exfoliation in liquids, Nat. Mater. 13 (2014) 624–630, https://doi.org/10.1038/nmat3944.

[10] J.M. Tour, Layered materials: scaling up exfoliation, Nat. Mater. 13 (2014) 545–546, https://doi.org/10.1038/nmat3961.

[11] Y. Xu, H. Cao, Y. Xue, B. Li, W. Cai, Liquid-phase exfoliation of graphene: an overview on exfoliation media, techniques, and challenges, Nanomaterials 8 (11) (2018), https://doi.org/10.3390/nano8110942, 942(1-32).

[12] X. Gu, Y. Zhao, K. Sun, C.L.Z. Vieira, Z. Jia, S. Huang, et al., Method of ultrasound-assisted liquid-phase exfoliation to prepare graphene, Ultrason. Sonochem. 58 (12) (2019), 104630, https://doi.org/10.1016/j.ultsonch.2019.104630.

[13] A.S. Mostovoy, A.V. Yakovlev, Reinforcement of epoxy composites with graphite-graphene structures, Sci. Rep. 9 (9) (2019), 16246, https://doi.org/10.1038/s41598-019-52751-z.

[14] L. Huang, Y. Huang, J. Liang, Y. Chen, Graphene-based conducting inks for direct inkjet printing of flexible conductive patterns and their applications in electric circuits and chemical sensors, Nano Res. 4 (2011) 675–684, https://doi.org/10.1007/s12274-011-0123-z.

[15] M. Yi, Z. Shen, S. Liang, L. Liu, X. Zhang, S. Ma, Water can stably disperse liquid-exfoliated graphene, Chem. Commun. 49 (2013) 11059–11061, https://doi.org/10.1039/c3cc46457a.

[16] F. Torrisi, T. Hasan, W. Wu, Z. Sun, A. Lombardo, T.S. Kulmala, et al., Inkjet-printed graphene electronics, ACS Nano 6 (4) (2012) 2992–3006, https://doi.org/10.1021/nn2044609.

[17] J. Li, F. Ye, S. Vaziri, M. Muhammed, M.C. Lemme, M. Ostling, Efficient inkjet printing of graphene, Adv. Mater. 25 (2013) 3985–3992, https://doi.org/10.1002/adma.201300361.

[18] T. Wu, A. De Luca, Q. Zhong, X. Zhu, O. Ogbeide, D.S. Um, et al., Inkjet-printed CMOS-integrated graphene–metal oxide sensors for breath analysis, npj 2D Mater. Appl. 3 (42) (2019) 1–10, https://doi.org/10.1038/s41699-019-0125-3.

[19] L. Xu, Y. Wen, S. Pandit, V.R.S.S. Mokkapati, I. Mijakovic, Y. Li, et al., Graphene-based biosensors for the detection of prostate cancer protein biomarkers: a review, BMC Chem. 13 (112) (2019) 1–12, https://doi.org/10.1186/s13065-019-0611-x.

[20] H. Gu, H. Tang, P. Xiong, Z. Zhou, Biomarkers-based biosensing and bioimaging with graphene for cancer diagnosis, Nanomaterials 9 (130) (2019) 1–24, https://doi.org/10.3390/nano9010130.

[21] D. Selvakumar, H. Sivaram, A. Alsalme, A. Alghamdi, R. Jayavel, Freestanding flexible, pure and composite form of reduced graphene oxide paper for ammonia vapor sensing, Sci. Rep. 9 (8) (2018) 8749, https://doi.org/10.1038/s41598-019-45408-4.

[22] S. Kumar, A. Garg, ChowdhuriA, Comparison of water purification properties of graphene oxide (GO) membranes with tuned interlayer spacings, Mater. Res. Express 6 (1) (2018), https://doi.org/10.1088/2053-1591/aae416, 015604(9).

[23] J. Abraham, K.S. Vasu, C.D. Williams, K. Gopinadhan, Y. Su, C.T. Cherian, et al., Tunable sieving of ions using graphene oxide membranes, Nat. Nanotechnol. 12 (2017) 546–550, https://doi.org/10.1038/nnano.2017.21.

[24] W. Kong, H. Kum, S.H. Bae, J. Shim, H. Kim, L. Kong, et al., Path towards graphene commercialization from lab to market, Nat. Nanotechnol. 14 (2019) 927–938, https://doi.org/10.1038/s41565-019-0555-2.

[25] A. Ciesielski, P. Samorì, Graphene via sonication assisted liquid-phase exfoliation, Chem. Soc. Rev. 43 (2014) 381–398, https://doi.org/10.1039/C3CS60217F.

[26] M. Lotya, P.J. King, U. Khan, S. De, J.N. Coleman, High-concentration, surfactant-stabilized graphene dispersions, Nano 4 (6) (2010) 3155–3162, https://doi.org/10.1021/nn1005304.

[27] L.A. Belyaeva, P.M.G. Deursen, K.I. Barbetsea, G.F. Schneider, Hydrophilicity of graphene in water through transparency to polar and dispersive interactions, Adv. Mater. 30 (7) (2018), 1703274, https://doi.org/10.1002/adma.201703274.

[28] M. Buzaglo, M. Shtein, S. Kober, R. Lovrinčić, A. Vilan, O. Regev, Critical parameters in exfoliating graphite into graphene, Phys. Chem. Chem. Phys. 15 (2013) 4428–4435, https://doi.org/10.1039/c3cp43205j.

[29] P.G. Karagiannidis, S.A. Hodhe, L. Lombardi, F. Tomarchio, N. Decorde, S. Milana, Microfluidization of graphite and formulation of graphene-based conductive inks, ACS Nano 11 (3) (2017) 2742–2755, https://doi.org/10.1021/ascnano.6b07735.

[30] K.M.F. Shahil, A.A. Balandin, Graphene–multilayer graphene nanocomposites as highly efficient thermal interface materials, Nano Lett. 12 (2) (2012) 861–867, https://doi.org/10.1021/nl203906r.

[31] A.S. Wajid, S. Das, F. Irin, H.S.T. Ahmed, J.L. Shelburne, D. Parviz, et al., Polymer-stabilized graphene dispersions at high concentrations in organic solvents for composite production, Carbon 50 (2) (2012) 526–534, https://doi.org/10.1016/j.carbon.2011.09.008.

[32] H. Ma, Z. Shen, M. Yi, S. Ben, S. Liang, L. Liu, et al., Direct exfoliation of graphite in water with addition of ammonia solution, J. Colloid Interface Sci. 503 (2017) 68–75, https://doi.org/10.1016/j.jcis.2017.04.070.

[33] Z. Ismail, N.F.A. Kassim, A.H. Abdullah, A.S.Z. Abidin, F.D. Ismail, K. Yusoh, Black tea assisted exfoliation using a kitchen mixer allowing one-step production of graphene, Mater. Res. Express 4 (11) (2017), 075607, https://doi.org/10.1088/2053-1591/aa7ae2.

[34] V. Chabot, B. Kim, B. Sloper, C. Tzoganakis, A. Yu, Hyield production and purification of few layer graphene by Gum Arabic assisted physical sonication, Sci. Rep. 3 (7) (2013) 1378, https://doi.org/10.1038/srep01378.

[35] P. Turner, M. Hodnett, R. Doray, J.D. Carey, Controlled sonication as a route to in-situ graphene flake size control, Sci. Rep. 9 (8) (2019) 8710, https://doi.org/10.1038/s41598-019-45059-5.

[36] F.M. Fowkes, W.D. Harkins, The state of monolayers adsorbed at the interface solid - aqueous solution, J. Am. Chem. Soc. 62 (1940) 3377–3386, https://doi.org/10.1021/ja01869a029.

[37] Z. Li, Y. Wang, A. Kozbial, G. Shenoy, F. Zhou, H. Liu, et al., Effect of airborne contaminants on the wettability of supported graphene and graphite, Nat. Mater. 12 (10) (2013) 925–931, https://doi.org/10.1038/nmat3709.

[38] K.B. Ricardo, A. Sendecki, H. Liu, Surfactant-free exfoliation of graphite in aqueous solutions, Chem. Commun. (J. Chem. Soc. Sect. D) 50 (2014) 2751–2754, https://doi.org/10.1039/C3CC49273G.

[39] J. Kim, S. Kwon, D.H. Cho, B. Kang, H. Kwon, Y. Kim, et al., Direct exfoliation and dispersion of two-dimensional materials in pure water via temperature control, Nat. Commun. 6 (9) (2015) 8294, https://doi.org/10.1038/ncomms9294.

[40] S. Barwich, U. Khan, J.N. Coleman, A technique to pretreat graphite which allows the rapid dispersion of defect-free graphene in solvents at high concentration, J. Phys. Chem. C 117 (37) (2013) 19212–19218, https://doi.org/10.1021/jp4047006.

[41] J.H. Ding, H.R. Zhao, H.B. Yu, A water-based green approach to large-scale production of aqueous compatible graphene nanoplatelets, Sci. Rep. 8 (8) (2018) 5567, https://doi.org/10.1038/s41598-018-23859-5.

[42] G. Bepete, E. Anglaret, L. Ortolani, V. Morandi, K. Huang, A. Penicaud, et al., Surfactant-free single-layer graphene in water, Nat. Chem. 9 (2017) 347–352, https://doi.org/10.1038/nchem.2669.

[43] S. Pilli, P. Bhunia, S. Yan, R.J. LeBlanc, R.D. Tyagi, R.Y. Surampalli, Ultrasonic pretreatment of sludge: a review, Ultrason. Sonochem. 18 (2011) 1–18, https://doi.org/10.1016/j.ultsonch.2010.02.014.

[44] I. Tzanakis, D.G. Eskin, A. Georgoulas, D.K. Fytanidis, Incubation pit analysis and calculation of the hydrodynamic impact pressure from the implosion of an acoustic cavitation bubble, Ultrason. Sonochem. 21 (2) (2014) 866–878, https://doi.org/10.1016/j.ultsonch.2013.10.003.

[45] Y. Wang, G.S.B. Lebon, I. Tzanakis, Y. Zhao, K. Wang, J. Stella, et al., Experimental and numerical investigation of cavitation-induced erosion in thermal sprayed single splats, Ultrason. Sonochem. 52 (2019) 336–343, https://doi.org/10.1016/j.ultsonch.2018.12.008.

[46] Z. Shen, J. Li, M. Yi, X. Zhang, S. Ma, Preparation of graphene by jet cavitation, Nanotechnology 22 (36) (2011) 1–7, https://doi.org/10.1088/0957-4484/22/36/365306.

[47] E.B. Flint, K.S. Suslick, The temperature of cavitation, Science 253 (1991) 1397–1399, https://doi.org/10.1126/science.253.5026.1397.

[48] J. Han, J. Jang, H. Kim, J.Y. Hwang, H.K. Yoo, J.S. Woo, et al., Extremely efficient liquid exfoliation and dispersion of layered materials by unusual acoustic cavitation, Sci. Rep. 4 (7) (2015) 5133, https://doi.org/10.1038/srep05133.

[49] I. Tzanakis, G.S.B. Lebon, D.G. Eskin, K.A. Pericleous, Characterisation of the ultrasonic acoustic spectrum and pressure field in aluminium melt with an advanced cavitometer, J. Mater. Process. Technol. 229 (2016) 582–586, https://doi.org/10.1016/j.jmatprotec.2015.10.009.

[50] T.G. Leighton, The Acoustic Bubble, Academic Press, London, 1994, p. 613.

[51] I. Tzanakis, M. Hodnett, G.S.B. Lebon, N. Dezhkunov, D.G. Eskin, Calibration and performance assessment of an innovative high-temperature cavitometer, Sens. Actuators, A 240 (2016) 57–69, https://doi.org/10.1016/j.sna.2016.01.024.

[52] S. Haar, M.E.L. Gemayel, Y. Shin, G. Melinte, M.A. Squillaci, O. Ersen, et al., Enhancing the liquid-phase exfoliation of graphene in organic solvents upon addition of n-octylbenzene, Sci. Rep. 5 (9) (2015), 16684, https://doi.org/10.1038/srep16684.

[53] P. He, C. Zhou, S. Tian, J. Sun, S. Yang, G. Ding, et al., Urea-assisted aqueous exfoliation of graphite for obtaining high-quality graphene, Chem. Commun. 51 (22) (2015) 4651–4654, https://doi.org/10.1039/c5cc00059a.
[54] A.C. Ferrari, J.C. Meyer, V. Scardaci, C. Casiraghi, M. Lazzeri, F. Mauri, et al., Raman spectrum of graphene and graphene layers, Phys. Rev. Lett. 97 (4) (2006), 187401, https://doi.org/10.1103/PhysRevLett.97.187401.
[55] M.S. Dresselhaus, A. Jorio, F.A.G. Souza, R. Saito, Defect characterization in graphene and carbon nanotubes using Raman spectroscopy, Phil. Trans. Math. Phys. Eng. Sci. 368 (1932) (2010) 5355–5377, https://doi.org/10.1098/rsta.2010.0213.
[56] M.A. Pimenta, M.S. Dresselhaus, G. Dresselhaus, L.G. Cancado, A. Jorio, R. Saito, Studying disorder in graphite-based systems by Raman spectroscopy, Phys. Chem. Chem. Phys. 9 (2007) 1276–1290, https://doi.org/10.1039/b613962k.
[57] D.R. Cooper, B. D'Anjou, N. Ghattamaneni, B. Harack, M. Hilke, A. Horth, et al., Experimental review of graphene, ISRN Cond. Matter. Phys. 2012 (56) (2012), 501686, https://doi.org/10.5402/2012/501686.
[58] A. Eckmann, A. Felten, A. Mishchenko, L. Britnell, R. Krupke, K.S. Novoselov, et al., Probing the nature of defects in graphene by Raman spectroscopy, Nano Lett. 12 (8) (2012) 3925–3930, https://doi.org/10.1021/nl300901a.
[59] A.V. Tyurnina, H. Okuno, P. Pochet, J. Dijon, CVD graphene recrystallization as a new route to tune graphene structure and properties, Carbon 102 (2016) 499–505, https://doi.org/10.1016/j.carbon.2016.02.097.
[60] G.S.B. Lebon, I. Tzanakis, K.A. Pericleous, D.G. Eskin, P.S. Grant, Ultrasonic liquid metal processing: the essential role of cavitation bubbles in controlling acoustic streaming, Ultrason. Sonochem. 55 (2019) 243–255, https://doi.org/10.1016/j.ultsonch.2019.01.021.
[61] L.D. Rozenberg (Ed.), High Intensity Ultrasonic Fields, Nauka, Moscow, 1968 [Translated to English. 1971. New York: Plenum, 419].
[62] Z. Çiplak, N. Yildiz, A. Çalimli, Investigation of Graphene/Ag nanocomposites synthesis parameters for two different synthesis methods, Fullerenes, Nanotub. Carbon Nanostruct. 23 (4) (2014) 361–370, https://doi.org/10.1080/1536383X.2014.894025.
[63] V.G. Kravets, A.N. Grigorenko, R.R. Nair, P. Blake, S. Anissimova, K.S. Novoselov, et al., Spectroscopic ellipsometry of graphene and an exciton-shifted van Hove peak in absorption, Phys. Rev. B 81 (15) (2010), https://doi.org/10.1103/PhysRevB.81.155413, 155413(14).
[64] Q. Lai, S. Zhu, X. Luo, M. Zou, S. Huang, Ultraviolet-visible spectroscopy of graphene oxides, AIP Adv. 2 (5) (2012), 032146, https://doi.org/10.1063/1.4747817.
[65] M. Cheng, L. Huang, Y. Wang, J. Tang, Y. Wang, Y. Zhao, et al., Reduced graphene oxide–gold nanoparticle membrane for water purification, Separ. Sci. Technol. 54 (6) (2019) 1079–1085, https://doi.org/10.1080/01496395.2018.1525400.
[66] R.M.G. Boucher, Sonochemistry at low and high frequencies, Br. Chem. Eng. 15 (1970) 363–367.
[67] C. Backes, K.R. Paton, D. Hanlon, S. Yuan, M.I. Katsnelson, J. Houston, et al., Spectroscopic metrics allow in-situ measurement of mean size and thickness of liquid-exfoliated few-layer graphene nanosheets, Nanoscale 8 (7) (2016) 4311–4323, https://doi.org/10.1039/c5nr08047a.
[68] M. Minnaert, On musical air bubbles and sound of running water, Phila. Mag. 16 (7) (1933) 235–248, https://doi.org/10.1080/14786443309462277.
[69] G.S.B. Lebon, I. Tzanakis, K. Pericleous, D.G. Eskin, Experimental and numerical investigation of acoustic pressures in different liquids, Ultrason. Sonochem. 42 (2018) 411–421, https://doi.org/10.1016/j.ultsonch.2017.12.002.
[70] I. Tzanakis, G.S.B. Lebon, D.G. Eskin, K.A. Pericleous, Characterising the cavitation development and acoustic spectrum in various liquids, Ultrason. Sonochem. 34 (2017) 651–662, https://doi.org/10.1016/j.ultsonch.2016.06.034.
[71] C.D. Ohl, R. Ikink, Shock-wave-induced jetting of micron-size bubbles, Phys. Rev. Lett. 90 (21) (2003), https://doi.org/10.1103/PhysRevLett.90.214502, 214502(4).
[72] I. Tzanakis, D.G. Eskin, A. Georgoulas, D.K. Fytanidis, Incubation pit analysis and calculation of the hydrodynamic impact pressure from the implosion of an acoustic cavitation bubble, Ultrason. Sonochem. 21 (2) (2014) 866–878, https://doi.org/10.1016/j.ultsonch.2013.10.003.
[73] M.G. Sirotyuk, Experimental studies of ultrasonic cavitation, in: L.D. Rozenberg (Ed.), High-Intensity Ultrasonic Fields, Nauka, Moscow, 1968, pp. 169–220 (English translation: High Intensity Ultrasonic Fields. Plenum: New York; 1971).
[74] K. Yasuda, H. Matsushima, Y. Asakura, Generation and reduction of bulk nanobubbles by ultrasonic irradiation, Chem. Eng. Sci. 195 (2019) 455–461, https://doi.org/10.1016/j.ces.2018.09.044.
[75] T.H. Kim, H.Y. Kim, Distruptive bubble behaviour leading to microstructure damage in an ultrasonic field, J. Fluid Mech. 750 (2014) 355–371, https://doi.org/10.1017/jfm.2014.267.
[76] Q. Zeng, S.R. Gonzalea-Avila, R. Dijkink, P. Koukouvinis, M. Gavaises, C.D. Ohl, Wall shear stress from jetting cavitation bubbles, J. Fluid Mech. 846 (2018) 341–355, https://doi.org/10.1017/jfm.2018.286.
[77] J.A. Morton, M. Khavari, L. Qin, D.G. Eskin, J. Mi, I. Tzanakis, et al., New Insight into Sono-Exfoliation Mechanisms of Graphite Based on Novel In-Situ High-Speed Imaging Studies, Nat Comm, 2020. Submitted for publication.
[78] C. Petrier, M.F. Lamy, A. Francony, A. Benhacene, B. David, V. Renaudin, et al., Sonochemical degradation of phenol in dilute aqueous solutions: comparison of the reaction rates at 20 and 487 kHz, J. Phys. Chem. 98 (41) (1994) 10514–10520, https://doi.org/10.1021/j100092a021.
[79] Z. Lin, P.S. Karthik, M. Hada, T. Nishikawa, Y. Hayashi, Simple technique of exfoliation and dispersion of multilayer graphene from natural graphite by ozone-assisted sonication, Nanomaterials 7 (6) (2017) 125, https://doi.org/10.3390/nano7060125, 10.